ev. Mexicana Astron. Astrof., 20, 55-66 (1990)

H_2O AND SiO MASER EMISSION IN OH/IR STARS

Y. Gómez[1,2], J.M. Moran[2], and L.F. Rodríguez[1,2]

Received 1990 January 11

RESUMEN

Hicimos una búsqueda de emisión maser de H_2O y SiO en 84 estrellas OH/IR con flujos de IRAS a 12, 25, y 60 μm. Detectamos cuatro nuevas fuentes de H_2O y ocho nuevas fuentes de SiO. También se utilizaron detecciones reportadas anteriormente en la literatura para determinar los porcentajes de estrellas OH/IR que muestran emisión maser de H_2O y SiO como una función del color [25–12]. Actualmente se cree que el color [25–12] es un indicador de edad. El análisis estadístico de los datos sugiere que el porcentaje de estrellas OH/IR con emisión maser de SiO disminuye conforme el color [25–12] aumenta. Modelos simples que describen la evolución temporal de las estrellas OH/IR sugieren que es alrededor de [25–12]$\simeq +0.2$ cuando cesa o disminuye de manera importante la pérdida de masa de la estrella. Por otro lado, el porcentaje de estrellas con emisión maser de H_2O disminuye significativamente a [25–12]$\simeq -0.2$, antes de que la pérdida de masa cese. Las razones por las cuales el porcentaje de objetos con emisión maser de H_2O cae tan tempranamente aún no se conocen.

ABSTRACT

We searched for H_2O and SiO maser emission in 84 OH/IR stars that have measured IRAS fluxes at 12, 25, and 60 μm. We detected four new H_2O sources and eight new SiO sources. We have used previous detections reported in the literature to determine the percentage of OH/IR stars with H_2O and SiO maser emission as a function of [25–12] color. The percentage of objects with detectable H_2O and SiO maser emission decreases with increasing [25–12] color. This color is believed to be an age indicator. The statistical analysis of the data suggests that the percentage of OH/IR stars with SiO maser emission decrease as the [25–12] color increases. Current models for the time evolution of OH/IR stars suggest that it is around [25–12]$\simeq +0.2$ that the mass loss ceases or decreases significantly. The percentage of OH/IR stars with H_2O maser emission decreases significantly at [25–12]$\simeq -0.2$, before mass loss ceases. The reasons for the early drop in H_2O maser percentage are not known.

Key words: **INFRARED SOURCES – MASERS – STARS-EVOLUTION – STARS-LATE-TYPE**

I. INTRODUCTION

Our knowledge of stellar evolution from the ed giant phase to the planetary nebula phase ıas increased significantly in the last years. At ›resent, it is believed that the OH/IR stars represent ın evolutionary stage preceding that of planetary ıebula (Engels *et al.* 1983). The OH/IR stars are ocated at the top of the Asymptotic Giant Branch AGB) with typical mass loss rates of 10^{-5} $M_\odot$ yr^{-1} Baud and Habing 1983). The OH/IR stars have ›xygen-rich circumstellar shells, vary over long ›eriods (500-2000 days) and show double-peaked .612 MHz OH maser profiles. Usually they do not have optical counterparts, and most of their luminosity is in the infrared region. Most OH/IR stars have an IRAS source counterpart, and it is possible to place the OH/IR stars in IRAS color-color diagrams. Olnon *et al.* (1984) found a continuous sequence from classical Mira variables to the reddest OH/IR stars in the [60–25] versus [25–12] diagram. The color $[\lambda_1 - \lambda_2]$ is defined as log $[\lambda_2 F_1/\lambda_1 F_2]$, where λ_i is the wavelength and F_i is the flux density. This continuous sequence has been interpreted to have an evolutionary origin (Olnon *et al.* 1984; Bedijn 1987; Habing, van der Veen, and Geballe 1987; van der Veen and Habing 1988), in the sense that the more evolved OH/IR stars appear in the upper right side of the diagram. The coolest objects are in this region.

It is also known that the OH, H_2O and SiO ma-

. Instituto de Astronomía, UNAM.
:. Harvard-Smithsonian Center for Astrophysics.

sers appear stratified in the envelopes of late type stars. The location of the SiO masing region is closest to the stellar surface, at $R_{SiO} \sim 3\times10^{14}$cm, the H_2O masers occur farther out at $R_{H_2O} \sim 3\times10^{15}$cm, and the OH masers usually come from comparatively large distances from the star, at $R_{OH} \sim 3\times10^{16}$cm (Bowers 1985; Chapman and Cohen 1986). The stratification is due to both chemical and excitation conditions (Elitzur 1981).

On an intuitive level one would expect that, as the massive wind turns on, the SiO maser wil appear first, followed by H_2O and finally by OH. By a similar argument, when the massive wind turns of and the object is very close to become a planetary nebula, one would expect the different masers to disappear in the same order. Lewis (1989) proposes a much more detailed scheme for the evolution o the maser emission. In his description, the main lines of OH (at 1665 and 1667 MHz) disappear first to be followed by H_2O and eventually by SiO.

TABLE 1

POSITIONS AND IRAS FLUXES

No.	Source	α(1950)	δ(1950)	F(12) (Jy)	F(25) (Jy)	F(60) (Jy)	F(100) (Jy)
1	I00171+6542	$00^h17^m07^s.0$	65°42′ 54″	26.0	37.0	8.0	≤6.0
2	OH138.0+7.3	03 20 41.6	65 21 31	95.50	134.28	37.67	9.91
3	I05131+4530	05 13 06.6	45 30 48	26.0	54.0	14.0	3.3
4	OH231.8+4.2	07 39 59.0	−14 35 42	19.0	226.0	548.0	292.0
5	OH349.2-0.2	17 15 04.2	−37 54 53	2.51	19.77	104.71	≤529.66
6	0H349.8-0.3	17 16 50.2	−37 36 35	9.8	37.0	47.8	≤280.0
7	OH0.1+5.1	17 23 22.6	−26 02 25	3.7	10.6	7.1	≤7.8
8	I17256+0504	17 25 40.0	05 04 42	17.0	17.0	3.5	2.1
9	I17308+0822	17 30 49.0	08 22 42	12.0	14.0	3.5	≤2.0
10	I17317-3331	17 31 44.4	−33 31 34	104.0	290.0	234.0	≤735.0
11	I17359-2902	17 35 57.1	−29 02 28	2.0	12.3	7.6	≤263.0
12	OH0.9+1.3	17 39 23.8	−27 27 05	1.84	17.86	36.98	≤85.51
13	OH13.1+5.1	17 52 53.7	−15 03 20	10.28	20.51	7.87	≤27.04
14	OH2.2-1.7	17 54 05.0	−27 53 57	1.4	14.2	25.6	≤337.0
15	OH8.0+1.4	17 55 04.1	−21 20 54	5.4	21.0	30.7	≤43.4
16	I18011-1847	18 01 06.2	−18 47 21	2.54	13.68	16.29	≤60.26
17	I18069+0911	18 06 55.5	09 11 40	68.55	61.94	10.76	4.21
18	OH12.8+0.9	18 07 11.1	−17 27 13	23.77	76.56	83.18	≤304.79
19	I18076+3445	18 07 37.7	34 45 40	31.92	27.04	5.25	1.92
20	OH15.4+1.9	18 08 43.3	−14 40 40	2.58	21.88	32.21	≤216.77
21	I18095+2704	18 09 30.9	27 04 28	45.29	125.89	27.80	5.65
22	I18123+0511	18 12 21.7	05 11 56	10.76	11.07	4.21	≤1.85
23	OH15.7+0.8	18 13 34.5	−14 56 19	31.05	124.74	157.04	≤428.55
24	OH12.8-0.9	18 13 55.3	−18 16 09	11.59	16.90	13.93	≤298.40
25	OH20.8+3.1	18 15 12.5	−09 19 44	14.45	38.73	15.28	≤39.08
26	OH12.8-1.9	18 17 40.4	−18 48 33	54.45	80.17	23.55	≤147.23
27	OH16.1-0.3	18 18 14.4	−15 04 50	22.08	21.48	6.49	≤304.79
28	OH18.3+0.4	18 19 53.4	−12 49 17	15.56	42.46	34.04	≤44.06
29	I18231+0855	18 23 10.5	08 55 02	4.79	3.44	0.67	≤1.64
30	I18237+2150	18 23 42.8	21 50 23	6.92	5.97	0.82	≤1.00
31	OH20.8+0.5	18 24 37.8	−10 32 18	2.2	20.2	50.0	≤392.0
32	I18254+0750	18 25 26.0	07 50 24	5.6	6.9	1.4	≤4.0
33	OH21.5+0.5	18 25 43.0	−10 00 16	46.13	120.23	115.88	≤319.15
34	OH20.7+0.1	18 25 44.7	−10 52 52	12.36	37.67	61.38	≤251.19
35	OH19.2-1.0	18 26 40.9	−12 39 55	14.8	32.7	20.0	≤195.0
36	OH20.4-0.3	18 26 48.8	−11 17 57	12.36	30.48	18.71	≤291.07

TABLE 1 (CONTINUED)

No.	Source	α(1950)	δ(1950)	F(12) (Jy)	F(25) (Jy)	F(60) (Jy)	F(100) (Jy)
37	OH23.7+1.2	18 27 24.0	−07 38 57	56.49	62.52	15.14	≤72.44
38	OH17.7-2.0	18 27 40.0	−14 31 05	22.7	131.83	120.23	38.73
39	OH22.0-0.6	18 30 52.1	−10 00 23	3.25	8.79	19.23	56.49
40	OH24.7+0.2	18 32 47.8	−07 15 39	44.46	80.91	94.62	172.19
41	OH26.5+0.6	18 34 52.3	−05 26 37	395.75	630.96	461.32	≤310.46
42	OH25.1-0.3	18 35 33.3	−07 12 33	1.72	14.32	31.05	≤159.96
43	OH25.5-0.3	18 36 09.0	−06 47 37	14.8	34.1	88.5	≤183.0
44	OH27.5-0.9	18 42 01.6	−05 12 25	1.04	26.79	26.30	≤237.68
45	OH30.7+0.4	18 43 16.9	−01 49 57	25.12	52.48	48.31	212.81
46	OH26.4-2.0	18 43 46.1	−06 43 50	46.13	66.07	18.71	≤185.35
47	OH32.1+0.9	18 44 04.5	−00 20 32	8.09	13.06	8.24	≤288.40
48	OH27.8-1.5	18 44 57.7	−05 14 29	25.12	29.92	7.52	≤121.34
49	OH30.1-0.7	18 46 03.3	−02 54 01	110.66	280.54	237.68	≤809.10
50	OH30.4-0.7	18 46 43.7	−02 38 19	5.6	37.5,	57.3	≤221.0
51	OH34.7+0.9	18 48 43.9	01 52 41	29.65	31.33	8.63	≤233.35
52	OH32.0-0.5	18 48 50.8	−01 07 32	16.44	42.85	44.06	73.11
53	OH40.1+2.4	18 53 31.5	07 26 31	63.10	70.47	11.48	≤84.72
54	OH35.6-0.3	18 54 55.3	02 08 08	13.06	28.05	23.12	77.98
55	OH37.1-0.9	18 59 36.3	03 15 52	2.61	14.19	22.49	≤112.72
56	OH39.9+0.0	19 01 42.4	06 08 39	16.44	31.05	13.43	≤95.50
57	OH42.6+0.0	19 06 34.3	08 32 55	20.14	51.52	31.05	≤122.46
58	0H42.3-0.1	19 06 42.8	08 11 38	24.66	71.78	38.73	≤91.20
59	OH43.8+0.5	19 07 08.8	09 46 53	7.94	18.03	5.60	≤85.51
60	I19172+1956	19 17 17.4	19 56 02	4.88	7.05	2.51	≤6.79
61	OH44.8-2.3	19 19 13.1	09 22 07	127.06	155.60	41.30	9.82
62	OH52.4+1.8	19 19 18.3	18 04 25	0.53	9.12	15.85	≤58.61
63	I19200+1536	19 20 01.5	15 36 00	6.08	10.76	5.15	≤41.30
64	I19201+2101	19 20 05.0	21 01 30	10.9	27.0	12.0	≤8.0
65	VY2-2	19 21 59.1	09 47 58	15.42	93.76	42.46	10.28
66	OH51.8-0.2	19 25 26.4	16 31 12	16.6	44.87	36.31	34.67
67	OH55.0+0.7	19 28 18.1	19 44 19	88.72	178.65	87.90	≤31.33
68	I19288+2923	19 28 51.4	29 23 34	40.55	57.02	13.68	7.24
69	OH57.5+1.8	19 29 37.7	22 27 17	31.62	41.69	13.18	≤8.63
70	I19386+1513	19 38 37.0	15 13 06	35.0	35.0	5.9	≤3.0
71	I19387+1527	19 38 46.0	15 27 12	6.2	7.0	1.5	-3.0
72	I19440+2251	19 44 01.0	22 52 00	15.0	30.0	14.0	≤9.0
73	I19459+1716	19 45 55.0	17 16 30	5.4	7.1	1.8	≤2.0
74	I19467+2213	19 46 43.0	22 13 42	2.3	3.7	0.9	≤4.0
75	OH65.4+1.3	19 49 21.6	29 05 18	22.28	34.36	5.97	≤6.92
76	I19534+2802	19 53 28.0	28 02 48	8.1	14.0	4.0	≤10.0
77	OH65.7-0.8	19 57 36.3	28 14 51	17.38	37.33	15.42	≤10.0
78	OH66.8-1.3	20 02 18.5	28 55 31	5.25	14.59	10.76	≤37.33
79	I20137+2838	20 13 44.0	28 38 36	4.1	9.3	2.6	≤4.0
80	I20160+2734	20 16 00.9	27 34 36	0.9	1.84	1.80	≤17.70
81	I20181+2234	20 18 11.0	22 34 15	25.59	32.81	6.73	≤9.55
82	OH75.3-1.8	20 27 12.5	35 35 35	11.59	33.42	35.65	25.59
83	OH83.4-0.9	20 49 09.5	42 36 47	54.95	69.82	15.56	≤16.90
84	OH104.9+2.4	22 17 43.1	59 36 16	123.59	229.09	90.35	34.99

In this paper we present the results of a survey of H_2O and SiO maser emission in a sample of 84 OH/IR stars. Our purpose was to study the statistics of H_2O and SiO maser emission as a function of IRAS colors.

II. SOURCE SELECTION AND OBSERVATIONS

The sample of OH/IR stars was obtained by use of the following criteria. We selected the 141 sources with measured IRAS fluxes at 12, 25, and 60 μm and with F(25 μm) $\geq$ F(12 μm) from the literature

TABLE 2

H_2O AND SiO MASERS IN SAMPLE

No.	Source	[25–12]	[60–25]	H_2O Det?	SiO Det?	Ref. H_2O	Ref. SiO
1	I00171+6542	−0.254	−1.081	NO	NO		
2	OH138.0+7.3	−0.259	−0.968	NO	YES		(1)
3	I05131+4530	−0.089	−1.002	NO	NO		
4	OH231.8+4.2	0.669	−0.031	YES	YES	(10)	(12)
5	OH349.2-0.2	0.490	0.308	NO	NO		
6	0H349.8-0.3	0.170	−0.305	NO	NO		
7	OH0.1+5.1	0.050	−0.590	NO	NO		
8	I17256+0504	−0.407	−1.102	YES	NO	(4)	
9	I17308+0822	−0.340	−1.018	NO	NO		
10	I17317-3331	0.039	−0.509	NO	NO		
11	I17359-2902	0.382	−0.625	NO	NO		
12	OH0.9+1.3	0.580	−0.100	NO	NO		
13	OH13.1+5.1	−0.107	−0.832	NO	YES		(6)
14	OH2.2-1.7	0.599	−0.160	NO	NO		
15	OH8.0+1.4	0.183	−0.251	NO	NO		
16	I18011-1847	0.315	−0.346	NO	NO		
17	I18069+0911	−0.451	−1.176	YES	NO	(4)	
18	OH12.8+0.9	0.101	−0.380	NO	NO		
19	I18076+3445	−0.479	−1.128	YES	YES	(4)	(9)
20	OH15.4+1.9	0.522	−0.248	NO	NO		
21	I18095+2704	0.037	−1.072	NO	NO		
22	I18123+0511	−0.394	−0.836	NO	NO		
23	OH15.7+0.8	0.197	−0.316	YES	YES	(5)	(6)
24	OH12.8-0.9	−0.243	−0.500	YES	NO	(5)	
25	OH20.8+3.1	0.021	−0.820	NO	NO		
26	OH12.8-1.9	−0.239	−0.948	YES	YES	(7)	(9)
27	OH16.1-0.3	0.010	−0.328	YES	YES	(9)	
28	OH18.3+0.4	0.029	−0.512	NO	NO		
29	I18231+0855	−0.551	−1.126	YES	NO	(4)	
30	I18237+2150	−0.471	−1.278	NO	NO		
31	OH20.8+0.5	0.556	−0.022	NO	NO		
32	I18254+0750	−0.316	−1.109	NO	NO		
33	OH21.5+0.5	0.010	−0.434	NO	YES		(6)
34	OH20.7+0.1	0.077	−0.204	NO	NO		
35	OH19.2-1.0	−0.063	−0.629	NO	YES		(6)
36	OH20.4-0.3	−0.015	−0.628	NO	NO		
37	OH23.7+1.2	−0.363	−1.032	NO	NO		
38	OH17.7-2.0	0.357	−0.456	YES	NO	(2)	
39	OH22.0-0.6	0.025	−0.076	NO	NO		
40	OH24.7+0.2	−0.147	−0.348	YES	YES	(9)	

TABLE 2 (CONTINUED)

No.	Source	[25–12]	[60–25]	H_2O Det?	SiO Det?	Ref. H_2O	Ref. SiO
41	OH26.5+0.6	−0.204	−0.552	YES	YES	(2)	(1)
42	OH25.1-0.3	0.514	−0.080	NO	NO		
43	OH25.5-0.3	−0.044	−0.002	NO	NO		
44	OH27.5-0.9	1.004	−0.424	NO	NO		
45	OH30.7+0.4	−0.087	−0.452	YES	YES	(3)	(9)
46	OH26.4-2.0	−0.251	−0.964	NO	YES		(6)
47	OH32.1+0.9	−0.199	−0.616	NO	NO		
48	OH27.8-1.5	−0.331	−1.016	NO	NO		
49	OH30.1-0.7	−0.003	−0.488	YES	YES	(8)	(1)
50	OH30.4-0.7	0.419	−0.232	NO	NO		
51	OH34.7+0.9	−0.383	−0.976	YES	NO	(9)	
52	OH32.0-0.5	0.009	−0.404	NO	NO		
53	OH40.1+2.4	−0.359	−1.204	YES	NO	(4)	
54	OH35.6-0.3	−0.075	−0.500	NO	NO		
55	OH37.1-0.9	0.329	−0.216	YES	YES	(9)	(6)
56	OH39.9+0.0	−0.131	−0.780	NO	YES		(6)
57	OH42.6+0.0	0.001	−0.636	NO	NO		
58	0H42.3-0.1	0.057	−0.684	YES	YES	(3)	(6)
59	OH43.8+0.5	−0.051	−0.924	YES	NO	(5)	
60	I19172+1956	−0.247	−0.864	NO	NO		
61	OH44.8-2.3	−0.319	−0.992	YES	YES	(5)	(9)
62	OH52.4+1.8	0.829	−0.176	NO	NO		
63	I19200+1536	−0.159	−0.736	NO	NO		
64	I19201+2101	−0.013	−0.768	NO	NO		
65	VY2-2	0.377	−0.760	NO	NO		
66	OH51.8-0.2	0.025	−0.508	NO	NO		
67	OH55.0+0.7	−0.103	−0.724	NO	NO		
68	I19288+2923	−0.259	−1.036	YES	YES	(4)	(9)
69	OH57.5+1.8	−0.287	−0.916	NO	NO		
70	I19386+1513	−0.407	−1.189	YES	YES	(4,11)	(9)
71	I19387+1527	−0.354	−1.085	YES	NO	(11)	
72	I19440+2251	−0.106	−0.747	NO	NO		
73	I19459+1716	−0.288	−1.012	NO	NO		
74	I19467+2213	−0.200	−1.030	YES	NO	(11)	
75	OH65.4+1.3	−0.219	−1.176	YES	YES	(5)	(6)
76	I19534+2802	−0.169	−0.960	NO	NO		
77	OH65.7-0.8	−0.075	−0.800	NO	NO		
78	OH66.8-1.3	0.037	−0.548	NO	NO		
79	I20137+2838	−0.051	−0.969	YES	NO	(4)	
80	I20160+2734	−0.096	−0.425	NO	NO		
81	I20181+2234	−0.299	−1.104	NO	NO		
82	OH75.3-1.8	0.053	−0.388	NO	NO		
83	OH83.4-0.9	−0.303	−1.068	YES	NO	(2)	
84	OH104.9+2.4	−0.139	−0.820	YES	YES	(2)	(1)

(1) Jewell *et al.* 1984. (2) Nyman, Johansson, and Booth 1986. (3) Olnon *et al.* 1980. (4) Lewis and Engels, 1988. (5) Engels, Schmid-Burk, and Walmsley 1986. (6) Jewell *et al.* 1985. (7) Marques dos Santos, Lépine, and Gomez-Balboa 1979. (8) Cato *et al.* 1976. (9) This paper. (10) Morris and Knapp 1976. (11) Engels *et al.* 1984. (12) Barvainis and Clemens 1984.

(Baud *et al.* 1979; Bowers 1978; Johansson *et al.* 1977; Pottasch, Bignell, and Zijlstra 1987; Baud *et al.* 1981; Lewis, Eder, and Terzian 1985; Sivagnanam and Le Squeren 1986; Seaquist and Davis 1983; te Lintel Hekkert *et al.* 1989). This last criterion was adopted because we were interested in studying the coolest objects, supposedly the ones that are close to the transition to the planetary nebula phase. The 100 μm fluxes were not used in the present analysis because of the problem of confusion given the location of most sources near the galactic plane. Objects identified as H II regions or with large negative declinations ($\delta \leq -38°$) were also excluded. In particular, we have excluded OH 5.89–0.3 (Zijlstra and Pottasch 1988) since its IRAS fluxes and colors, as well as its association with an H_2O maser source and a highly excited ammonia source (Gómez *et al.* 1990) strongly suggest that it is a compact H II region. We arrived at a final sample size of 84 stars.

The H_2O (22.2 GHz) and SiO (43.1 GHz) observations of the 84 stars were made at the IRAS positions (Table 1) using the 36.6-m antenna of the Haystack Observatory[3] in three sessions during July 1988, October 1988, and March 1989. At the observing frequencies, the half power beam width and aperture efficiency at an elevation of 45° of the antenna were 1.′5 and 0.28 (22.2 GHz) and 0.′8 and 0.11 (43.1 GHz). The rms pointing accuracy was estimated to be $\sim 10''$. As a spectrometer we used a 512-channel digital autocorrelator with a total bandwidth of 16.67 MHz, giving a velocity resolution (unity weighting) of 0.53 km s^{-1} for the H_2O observations and 0.27 km s^{-1} for the SiO observations. The observations were made in the total power mode, with total integration times of 10 minutes. The 84 stars in our sample were typically observed four to eight times for a total on-source integration time of 20 to 40 minutes. All spectra were corrected for atmospheric attenuation and elevation-dependent gain variations. The rms flux densities in the final spectra were in the range of 0.5 to 2.0 Jy for the H_2O observations and in the range of 1.5 to 9.0 Jy for the SiO observations.

III. RESULTS AND DISCUSSION

In Table 1 we show the positions and IRAS fluxes of the stars in our sample. We obtained the [25–12] and [60–25] colors for each source after applying the color correction factors for a blackbody at 300 K (Neugebauer *et al.* 1984) with the relations

$$[25-12] = log\left(\frac{12\ F(25)\ (0.89)}{25\ F(12)\ (1.09)}\right)$$

$$[60-25] = log\left(\frac{25\ F(60)\ (0.82)}{60\ F(25)\ (0.89)}\right).$$

In Table 2 we present a list of the [25–12] and [60–25] colors of the stars in our sample as well as information about whether or not H_2O and SiO masers have been detected and the respective references. We also made a [60–25] versus [25–12] diagram (see Figure 1) with our 84 OH/IR stars. To check that our sample is not biased in the sense that objects with different colors may have different integrated IRAS fluxes, we show in Figure 2 a diagram of IRAS luminosity (assuming that the sources are at 1 kpc) versus [25–12] color. This is equivalent to plotting integrated flux versus color. As can be seen, there is no obvious bias.

i) H_2O Masers

We detected 14 H_2O masers in the sample, of which 4 are new detections. The parameters of the new masers are given in Table 3 and their spectra are shown in Figure 3. Combining our results with previous detections in the literature (see references in Table 2) we find that 28 of the 84 stars are associated with H_2O maser emission. In particular, we have considered OH 37.1–0.9 as an H_2O maser detection. The H_2O maser emission from this source was first observed by Engels, Schmid-Burgk and Walmsley (1986), who did not consider it to be associated with the OH/IR star because the H_2O radial velocity range (63 to 69 km s^{-1}) is outside that of the OH velocity range (74 to 103 km s^{-1}). However, H_2O maser emission features with radial velocities outside the range defined by the OH peaks is now known to the present in several late type stars (Bowers, Johnston, and De Vegt 1989). We believe that the observed H_2O maser is associated with OH 37.1–0.9.

TABLE 3

NEW H_2O DETECTIONS

Source	S_L^a (Jy)	V_{LSR} (km s^{-1})	Date of Observation
OH 16.1–0.3	6.3	37.7	88 Jul 2
OH 24.7+0.2	8.2,6.3,3.4	26.3,26.7,30.7	88 Jul 6
OH 34.7+0.9	2.2	39.6	88 Jul 2
OH 37.1–0.9	3.7	67.9	88 Jul 7

a. We assumed a sensitivity of 9.1 Jy/K.

3. Radio Astronomy at the Haystack Observatory of the Northeast Radio Observatory Corporation is supported by a grant from the National Science Foundation.

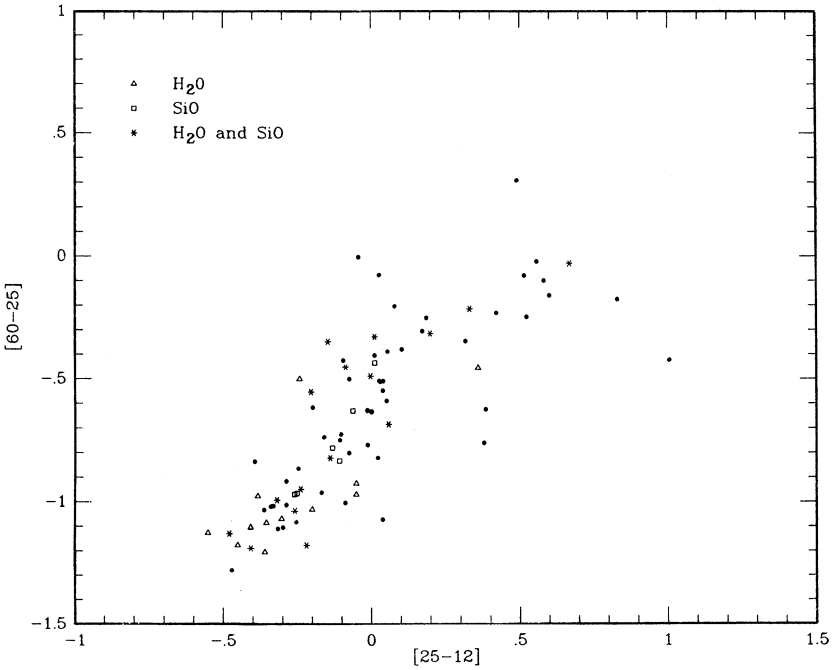

Fig. 1. The IRAS color-color diagram for the 84 OH/IR stars in our sample. The filled circles indicate the stars without SiO and H_2O maser emission. The asterisks indicate the stars with both H_2O and SiO emission. The triangles refer to those objects with only H_2O maser emission and the squares indicate the stars with only SiO maser emission.

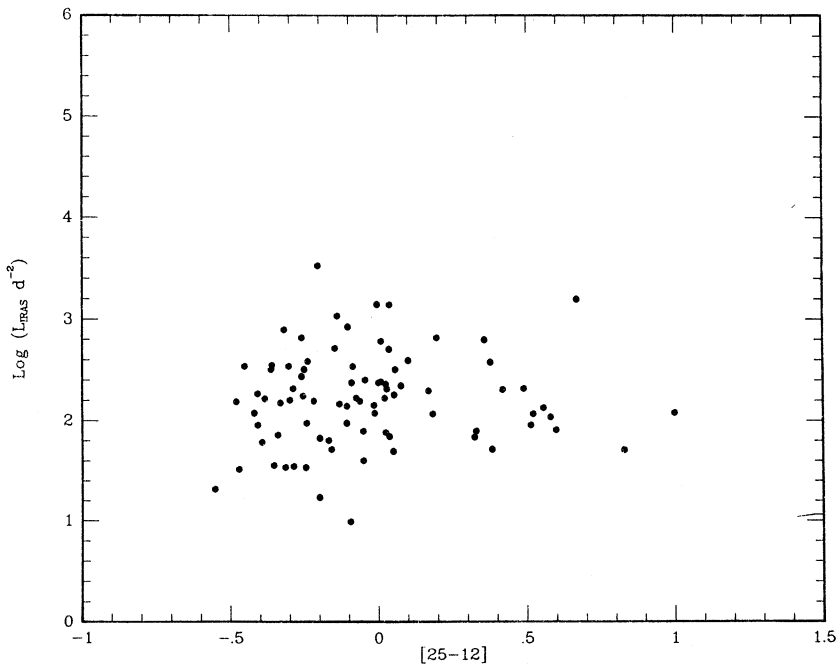

Fig. 2. The IRAS luminosity, calculated by placing all sources at 1 kpc, versus [25–12] color of the OH/IR stars of the sample.

ii) SiO Masers

We detected 13 SiO masers, of which 8 are new detections. The parameters of the new masers are given in Table 4 and their spectra are shown in Figure 4. Combining our results with previous detections in the literature (see references in Table 2), we find that 22 of the 84 stars are associated with SiO maser emission.

TABLE 4

NEW SiO DETECTIONS

Source	S_L^a (Jy)	V_{LSR} (km s^{-1})	Date of Observation
IRAS 18076+3445	9.0	4.2	88 Oct 15
OH 12.8–1.9	39.7	10.9	89 Mar 11
OH 16.1–0.3	51.0	22.0	89 Mar 12
OH 24.7+0.3	8.4,10.7	43.3,47.5	88 Aug 28
OH 30.7+0.4	14.8	68.9	89 Mar 11
OH 44.8–2.3	14.2	−71.6	89 Mar 11
IRAS 19288+2923	6.1	−37.8	89 Mar 11
IRAS 19386+1513	7.3	1.7	89 Mar 13

a. We assumed a sensitivity of 29 Jy/K.

iii) Interpretation

The color-color diagram for evolved stars has been interpreted as an evolutionary sequence from oxygen-rich Miras to OH/IR stars in the sense that it reflects an evolution in mass loss (Baud and Habing 1983; Bedijn 1987; van der Veen and Habing 1988). This IRAS color-color sequence has been modeled by Bedijn (1987). He used single dust shell models with optical depth increasing in time. The optical depth increases as the rate of mass loss increases. The IRAS color-color diagram also shows a "break" around [25–12]≃+0.2 (see Figure 1) that Bedijn (1987) suggests is caused by the cessation of mass loss. After that time, no more gas is added to the inner parts of the envelope and, as a whole, the envelope gets progressively cooler. In other words, the circumstellar envelope is now detached from the stellar surface and a cavity grows around the star.

We separated the 84 stars into three [25–12] color bins, −0.6 to −0.2 (28 stars), −0.2 to 0.2 (41 stars), and 0.2 to 1.0 (15 stars). The last bin is twice as large as the others in order to include a comparable number of stars. Figure 5 shows the percentage of objects that exhibit H_2O and SiO maser emission versus [25–12] color. The respective Poisson error is also shown. The percentages of

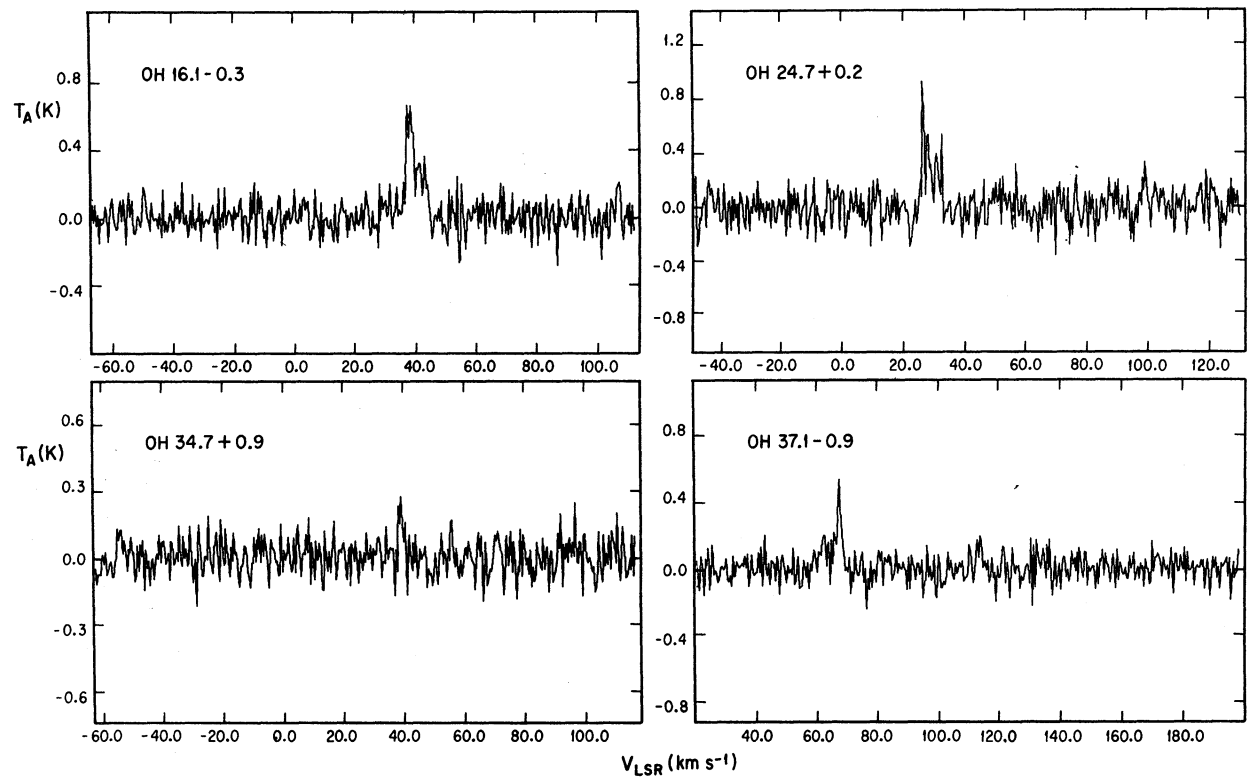

Fig. 3. Spectra of new detections of H_2O maser emission in our sample.

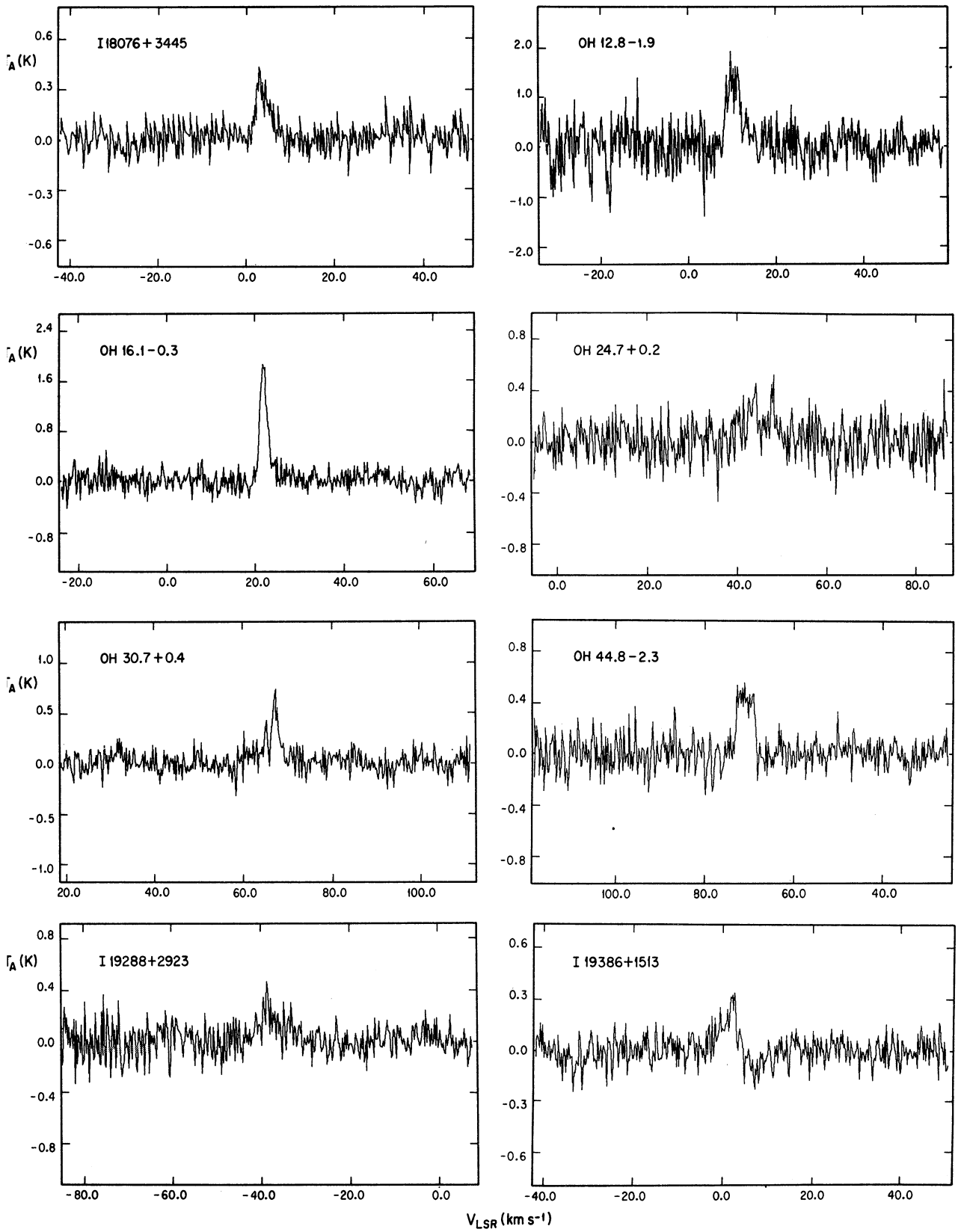

Fig. 4. Spectra of new detections of SiO maser emission in our sample.

both H_2O and SiO maser emission seem to decrease with increasing [25–12] color (see Figure 5). Using the chi-square test we determined the goodness of fit to the data for constant, linear, and step functions. This criterion clearly favors the step function as the best description of the H_2O data (see Table 5). The SiO data contains less detections and as a result the statistical analysis is less significant. In this case (see Table 5), the linear function is favored but the significance of the fit with a step function is similar.

TABLE 5

SIGNIFICANT (PERCENT) FROM THE CHI-SQUARE TEST

Function	H_2O (This paper)	SiO (This paper)	H_2O (Combined)
Constant	13	34	21
Linear	19	81	46
Step	78	71	86

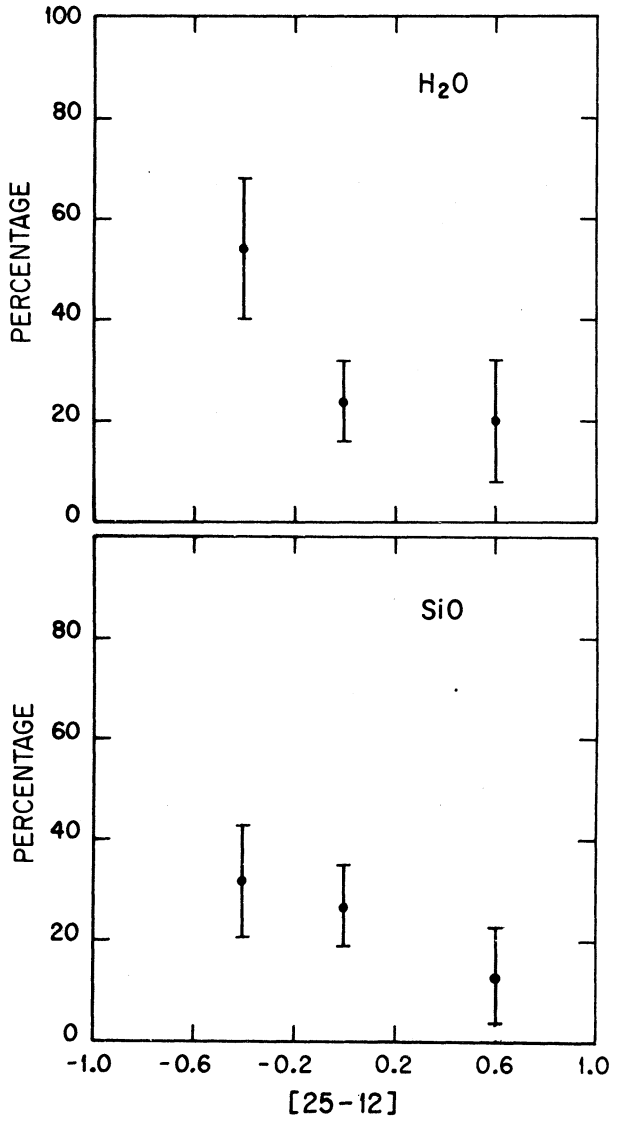

Fig. 5. Percentage of H_2O (above) and SiO (bottom) maser detections versus [25–12] color for the 84 OH/IR stars of our sample. The H_2O drop occurs at [25–12]$\simeq -0.2$. The SiO percentage seems to decrease more smoothly.

We searched for systematic bias in the distanc by plotting the galactic latitude of the stars versu their [25–12] colors. As can be seen in Figure 6 most stars are projected within a few degrees of th galactic plane. However, eight stars in the -0.6 t -0.2 color bin have large galactic latitudes ($b \geq 8°$) suggesting that they may be systematically closer However, the percentage of objects with H_2O maser emission in the high galactic latitude subsample (3 out of 8, or 38 ± 22 percent) is consistent within th errors with that of all sources in the color bin (1 out 28, or 54 ± 14 percent).

Similarly, the percentage of objects with SiO ma ser emission in the high galactic latitude subsampl (1 out of 8, or 13 ± 13 percent) is consistent withir the errors with that of all sources in the -0.6 to $-0.$ color bin (9 out of 28, or 32 ± 11 percent). We con clude that the inclusion of this high galactic latitud star does not affect the statistics significantly.

To improve the statistical significance of our H_2C maser analysis, we added to our sample additiona data from Eder, Lewis, and Terzian (1988). I their sample there are 156 additional OH/IR star

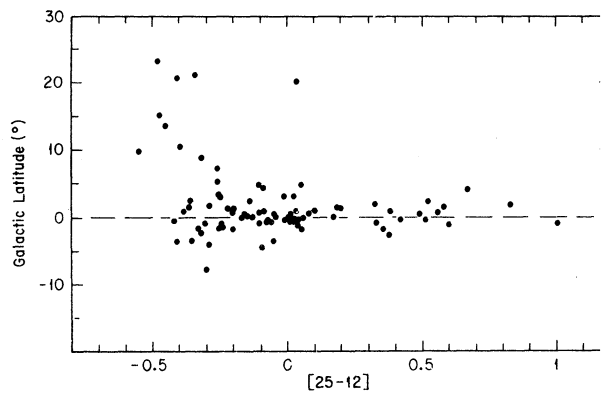

Fig. 6. Galactic latitude versus [25–12] color for the 8 OH/IR stars in our sample.

(generally with smaller [25–12] colors than the stars in our sample), with 44 of them having associated H_2O maser emission. The combined sample extends the [25–12] boundary to the left from −0.6 to −1.0. Figure 7 shows the percentage of sources that exhibits H_2O maser emission, using the combined sample. We separated the combined H_2O sample into four [2-5-12] color bins, −1.0 to 0.6 (10 stars), −0.6 to −0.2 (151 stars), −0.2 to 0.2 (61 stars), and 0.2 to 1.0 (18 stars). Applying the chi-square test to the combined sample we again determine that the better fit is a step function (see Table 5). Unfortunately, we could not find additional SiO data to improve the statistics for this molecule. In conclusion, we find that the best description of the H_2O data is in terms of a step function, although the significance is only modest, about 80 percent.

The adoption of a step function to describe the percentage of H_2O masers as a function of [25–12] color implies a characteristic [25–12] color where the percentage drops. For H_2O this occurs near [25–12]≃–0.2. Lewis (1989) reached a similar conclusion. If we think of a simple wind model, where the circumstellar envelope of the OH/IR star is expanding with a terminal velocity of ~10 km s^{-1}, and the SiO, H_2O, and OH masers are stratified in the envelope, it is then possible to calculate the time scale for the "disappearance" of each maser after mass loss stops. We obtain a time scale of 10, 100, and 1000 years for SiO, H_2O, and OH masers, respectively. Consequently if this simple model were actually describing the phenomenon, SiO maser emission would disappear first after steady mass loss has ceased, to be followed by H_2O and lastly by OH. From our results (see Figure 5) we find that the SiO maser emission decreases as the [25–12] color increases. However, the available data do not allow to conclude if the decrease is smooth or abrupt. More data is required to solve this problem. However, in the case of the H_2O maser emission we find that the percentage decreases abruptly *before* the mass loss ceases, with the drop occurring near [25–12] = −0.2.

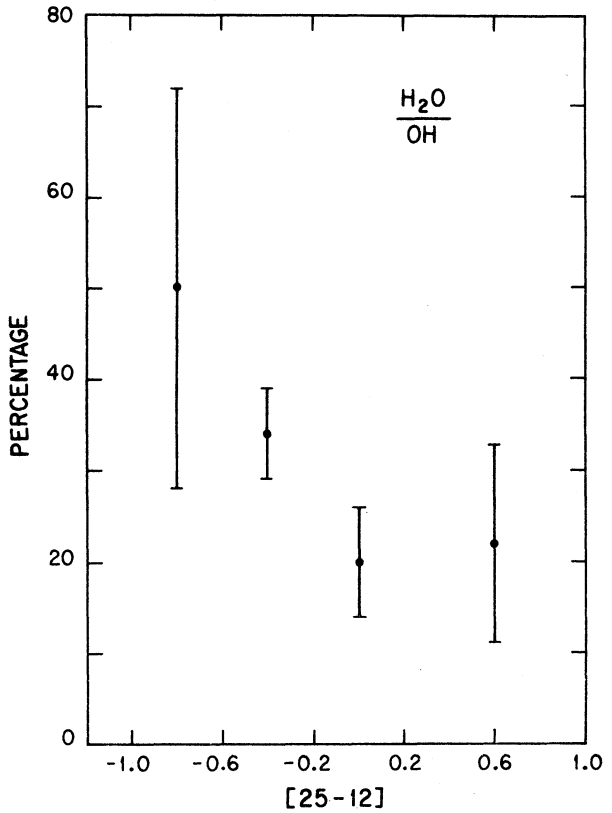

Fig. 7. Percentages for the combined H_2O sample (see text) versus [25–12] color. The drop in percentage also occurs at [25–12]≃ −0.2.

What then causes the drop in the percentage of H_2O masers? Deguchi (1977) proposed that stellar water masers may be pumped by collisional pocesses. Collisions with H_2 molecules could excite the vibrational ν_2 band of the H_2O molecule followed by a radiative decay at 6 μm. As the density increases (as a result of increase in the mass loss rate), collisional pumping becomes more effective. The inversion can occur as long as the gas is sufficiently dense and hot ($N_{H_2} \sim 10^{10}$ cm^{-3} and T~ 1000 K) (Deguchi 1977).

One possibility that can be easily ruled out is that the envelope reaches hydrogen densities large enough to quench the inversion required for the H_2O maser to work (e.g. the maser is thermalized by collisions). If we estimate the mass loss needed to get such large densities, 10^{10} cm^{-3}, using typical parameters (v = 10 km s^{-1}; $R_{H_2O} = 3\times10^{15}$ cm), we obtain a value for the mass loss rate (~6×10^{-2} $M_\odot$ yr^{-1}), several orders of magnitude larger than the expected values for a typical OH/IR star (~10^{-5} $M_\odot$ yr^{-1}). This result makes the quenching possibility unlikely.

Another possibility is that, with the increase in optical depth in the envelope, the region from which the H_2O maser originates becomes too cool for excitation of the levels involved in the maser emission. The models of Rowan-Robinson (1980) show that, for a given point in the outer parts of the envelope, an increase in optical depth produces a decrease in the temperature. Detailed modeling is required to establish whether or not the increase in optical depth with increasing mass loss produces a decrease in temperature large enough to inhibit the population of the levels in the H_2O molecules above maser transition.

IV. CONCLUSIONS

We present H_2O and SiO maser observations for 84 OH/IR stars made with the Haystack Observatory telescope. The main results of our study are summarized as follows.

1) We detected 14 H_2O masers and 13 SiO masers in the sample of 84 OH/IR stars. Four of the H_2O masers and eight of the SiO masers observed are new discoveries.

2) The percentages of OH/IR stars that exhibit H_2O and SiO maser emission decrease with increasing [25–12] color. This means that both H_2O and SiO maser emission disappear before the OH maser emission.

3) We find that the best description for the H_2O data is a step step function, although the significance is only modest, about 80 percent. For the H_2O masers we find that the percentage decreases abruptly around $[25–12] \simeq -0.2$, before the cessation of mass loss (which is believed to happen around $[25–12] \simeq +0.2$). The reasons for this early decrease are not evident to us. In the case of the SiO masers, more observations are required to establish the way in which the decrease takes place.

We thank C. Barret, P. Benson and I. Little-Marenin for their careful reading of the manuscript and an anonymous referee for comments and the suggestion of the galactic latitude test.

REFERENCES

Barvainis, R. and Clemens, D.P. 1984, ***A.J.***, **89**, 1833.
Baud, B., Habing, H. J., Matthews, H. E., and Winnberg, A. 1979, *Astr. and Ap. Suppl.*, **36**, 193.
Baud, B., Habing, H. J., Matthews, H. E., and Winnberg, A. 1981, *Astr. and Ap.*, **95**, 156.
Baud, B., Habing, H. J. 1983, *Astr. and Ap.*, **127**. 73.
Bedijn, P. J. 1987, *Astr. and Ap.*, **186**, 136.
Bowers, P. F. 1978, *Astr. and Ap.*, **64**, 307.
Bowers, P. F. 1985, in *Mass Loss from Red Giants*, ed. M. Morris and B. Zuckerman (Dordrecht: Reidel), p. 189.
Bowers, P. F., Johnston, K. J., and De Vegt, C. 1989, *Ap. J.*, 340, 479.
Cato, B. T. *et al.* 1976, *Ap. J.208, 87.*
Chapman, J. M. and Cohen, R. J. 1986, *M.N.R.A.S.*, **220**, 513.
Deguchi, S. 1977, *Pub. Astron. Soc. Japan*, **29**, 669.
Eder, J., Lewis, B. M., and Terzian, Y. 1988, *Ap. J. Suppl.*, **66**, 183.
Elitzur, M. 1981, in *Physical Processes in Red Giants*, ed. I. Iben and A. Renzini (Dordrecht: Reidel), p. 363.
Engels, D., Kreysa, E., Schultz, G. V., and Sherwood, W. A. 1983, *Astr. and Ap.*, **124**, 123.
Engels, D., Habing, H. J., Olnon, F. M., Schmid-Burgk, J., and Walmsley, C. M. 1984, *Astr. and Ap.*, 140, L9.
Engels, D., Schmid-Burgk, J., and Walmsley, C. M. 1986, *Astr. and Ap.*, **167**, 129.
Gómez, Y., Rodríguez, L. F., Garay, G., and Moran, J. M. 1990, in preparation.
Habing, H. J., van der Veen, W., and Geballe, T. 1987, in *Late Stages of Stellar Evolution*, ed. S. Kwok and S. R. Pottasch (Dordrecht: Reidel), p. 91.
Jewell, P. R., Batrla, W., Walmsley, C. M., and Wilson, T. L. 1984, *Astr. and Ap.*, **130**, L1.
Jewell, P. R., Walmsley, C. M., Wilson, T. L., and Snyder, L. E. 1985, *Ap. J. (Letters)*, **298**, L55.
Johansson, L. E. B., Andersson, C., Goss, W. M., and Winnberg, A. 1977, *Astr. and Ap. Suppl.*, **28**, 199.
Lewis, B. M., Eder, J., and Terzian, Y. 1985, *Nature*, **313**, 200.
Lewis, B. M. and Engels, D. 1988, *Nature*, **332**, 49.
Lewis, B. M. 1989, *Ap. J.*, **338**, 234.
Marques dos Santos, P., Lépine, J. R. D., Gomez-Balboa, A. M. 1979, *A.J.*, **84**, 787.
Morris, M. and Knapp, G. R. 1976, *Ap. J.*, **204**, 415.
Neugebauer, G. *et al.* 1984, *Ap. J. (Letters)*, **278**, L1.
Nyman, L. A., Johansson, L. E. B., and Booth, R. S. 1986, *Astr. and Ap.*, **160**, 352.
Olnon, F. M., Winnberg, A., Matthews, H. E., and Schultz, G. V. 1980, *Astr. and Ap. Suppl.*, **167**, 129.
Olnon, F. M. *et al.* 1984, *Ap. J.*, **278**, L41.
Pottasch, S. R., Bignell, C., and Zijlstra, A. 1987, *Astr. and Ap.*, **177**, L49.
Rowan-Robinson, M. 1980, *Ap. J. Suppl.*, **44**, 403.
Seaquist, E. R. and Davis, L. E. 1983, *Ap. J.*, **274**, 659.
Sivagnanam, P. and Le Squeren, A. M. 1986, *Astr. and Ap.*, **168**, 374.
te Lintel Hekkert, P., Versteege-Hensel, H., Habing, H.J., and Wiertz, M. 1989, *Astr. and Ap. Suppl.*, **78**, 399.
van der Veen, W. E. C. J. and Habing H. J. 1988, *Astr. and Ap.*, 194, 125.
Zijlstra, A. A. and Pottasch, S. R. 1988, *Astr. and Ap.*, **196**, L9.

Yolanda Gómez and Luis F. Rodríguez: Instituto de Astronomía, UNAM, Apartado Postal 70-264, 04510 México, D.F., México.

James M. Moran: Harvard-Smithsonian Center for Astrophysics, 60 Garden Street MS 42, Cambridge, MA 02138, USA.